J Mater Sci (2006) 41:5134–5145
DOI 10.1007/s10853-006-0439-3

Delamination under Hertzian cyclic loading of a glass coating on Ti6al4v for implants

J. Pavón · E. Jiménez-Piqué · M. Anglada · E. Saiz · A. P. Tomsia

Received: 29 September 2005 / Accepted: 17 January 2006 / Published online: 27 July 2006

Abstract In this work, the interfacial response of a glass-based coating on Ti6Al4V to monotonic and cyclic Hertzian (spherical) indentation is investigated. This coating belongs to the SiO_2-CaO-MgO-Na_2O-K_2O-P_2O_5 system and it is specifically designed to be used as the inner layer of a bioactive bilayer coating with an outer layer of lower SiO_2 content to ensure bioactivity. During Hertzian monotonic loading, delamination of the coating occurs, which is revealed in the microscope by the presence of a colour pattern of interference fringes at the interface. Hertzian cyclic loading at maximum loads, P_{max}, lower than the monotonic delamination load, P_{Del}, also generates delamination damage. A plot of P_{max} versus the number of cycles for delamination shows a two-slope curve with a ''knee'' for P_{max} close to the critical load to induce a radial crack from the interface, P_{Rc}. The analysis of the delamination morphology and the results for different load ratios, $R = P_{min}/P_{max}$, confirmed the existence of two different delamination mechanisms with a common feature of plastic deformation of the substrate but with a different dependence with the maximum applied load: for $P_{max} > P_{Rc}$ the process is mostly controlled by the presence of the radial cracks (P_{max} dependent), meanwhile, for $P_{max} < P_{Rc}$ radial cracks are not observed and delamination is attributed to the residual stress at the interface induced by the cyclic plastic deformation of the substrate and the elastic recovery of the coating during unloading part.

J. Pavón (✉) · E. Jiménez-Piqué · M. Anglada
Departament de Ciencia dels Materials i Enginyeria Metal.lúrgica, Universitat Politècnica de Catalunya, Avda. Diagonal 647 (ETSEIB), 08028 Barcelona, Spain
e-mail: juan.jose.pavon-palacio@upc.es

E. Saiz · A. P. Tomsia
Materials Sciences Division, Ernest Orlando Lawrence Berkeley National Laboratory, Berkeley, CA 94720, USA

Introduction

Bioactive materials are defined as those which, once implanted, form an interfacial bond with the tissue, preventing motion between the two parts and imitating the type of interface that is formed when natural tissues repair themselves [1]. The use of these materials as a coating for metallic implants has been proposed as an alternative for improving the interaction with the tissue and avoiding the formation of a non-adherent fibrous capsule around the implant [2]. Synthetic hydroxyapatite ($Ca_{10}(PO_4)_6(OH)_2$), similar to the mineral component of the bone, is the bioactive material most widely used to coat Ti alloys by plasma spraying and ion sputtering techniques [3, 4]. However, it has been observed that the major cause of failure of these coatings resides in the poor adhesion to the titanium substrate [5]. An alternative method is to coat the metallic implants with a bioactive glass that can precipitate hydroxyapatite in vivo, optimizing at the same time the adhesion to the substrate. Therefore, there have been attempts to coat metallic implants with this material, by using different techniques such as enamelling, glazing, rapid immersion in molten glass, flame-spray coating, or plasma-spraying techniques [6]. Although excellent in vitro behaviour has been obtained by some of these methods, most of the coatings fail

by cracking and show poor reliability of the glass/metal interface [7]. In many cases, interfacial reactions lead to the formation of brittle layers and gas bubbles in the coating [8].

Tomsia and co-workers (see references [9–11]) have developed a simple technique for applying improved bioactive coatings on Ti-based alloys, using glasses of the SiO_2-CaO-MgO-Na_2O-K_2O-P_2O_5 system. The chemical composition of these glasses is based on the Bioglass® developed by Hench et al. [12], with increased SiO_2 content, and partial substitution of the original K_2O and MgO with Na_2O and CaO, respectively. These changes were done in order to reduce the coating thermal expansion coefficient so that it is closer to that of the substrate. This coating is designed to be the primary layer in direct contact with the substrate, while an outer layer (lower SiO_2 content) will ensure the surface bioactivity and it will be dissolved once implanted [7].

Besides improving the interfacial bond with the hosting bone, a bioactive coating should response satisfactorily to the very complex mechanical requirements at the implant/tissue interface [13]. The most common and most severe involves resistance to concentrated forces from contacts of characteristic radius [14]. Previous works have shown that the Hertzian (spherical) indentation method is a powerful tool to simulate some biomechanical loading conditions, specifically the basic elements of occlusal [15] and part of the hip function [16]. Moreover, this method has inherent advantages for mechanical characterization because it can be implemented by means of a simple test configuration with small specimens and also because its suitability for measuring intrinsic mechanical properties.

The adhesion coating/implant is a very critical feature of the system in order to ensure its long-term mechanical stability. The aim of this work is, therefore, to determine the interfacial response of the glass coating to monotonic and cyclic Hertzian contact loading. The paper is arranged in the following sequence. A brief description of the microstructural features of the coating is presented in section Experimental procedure as well as the basic mechanical testing data. Section Hertzian indentation damage sequence in the coating in monotonic loading describes the damage sequence obtained during a monotonic test and the analysis of the interfacial damage. Delamination by cyclic loading followed by the analysis of the damage morphology and the influence of the load ratio, R, are presented in section Delamination due to the Hertzian cyclic loading. The paper concludes in section Conclusion with a summary of the salient findings of this work.

Experimental procedure

Preparation and characterization of the coatings

The starting glasses to prepare the coatings were obtained by mixing the appropriate reagents (SiO_2: 99.5%, Cerac; $CaCO_3$: 99.9%, JT Baker; MgO: 98.6%, JT Baker; K_2CO_3: 99.0%, Allied Chemical; $NaHCO_3$: 99.5%; JT Baker; and $NaPO_3$: 99.7% Allied chemical) in ethanol using a high-speed stirrer to achieve the desired composition for each glass (Table 1). The mixture was first dried at 80 °C for 12 h and then air-fired at temperatures ranging from 1400 °C to 1500 °C for 4 h in a Pt crucible. The melt was cast into a graphite mould to obtain glass plates (~50 × 50 × 5 mm) that were subsequently annealed at 500 °C for 6 h to relieve stresses and then milled in a planetary agate mill. Annealing was only strictly necessary to eliminate the residual stresses of the bulk glass samples, but not for the samples subsequently used to fabricate the coatings. To obtain the coatings, a suspension of the glass powder (particle size of 13 ± 2 μm [17]) in ethanol was deposited via sedimentation on Ti6Al4V beams (99.0% purity, 45 × 5 × 4 mm), which had been previously polished with diamond suspension (1 μm particle size) and cleaned in ultrasonic baths of acetone and ethanol. Afterwards, in order to sinter the glass powder, the coating was air-dried at 75 °C overnight and fired in a Unitek dental furnace by preheating to 600 °C in air followed by simultaneously evacuating the oven to 1.3×10^{-5} Pa and by using a high heating rate (40 °C/min) to the desired temperature (800–820 °C). Once the peak temperature was reached, the vacuum was released by the furnace and the coating was quenched in air. Further details of the experimental procedure can be found in references [9–11]. The initial beams were sectioned into samples of 5 × 3 × 4 mm to allow observation of the coating cross-section and performing indentation tests. The thickness of the coating, measured from observations of the cross-section by optical microscopy, was approximately 40 μm.

The first physical feature of the coating that can be observed by optical microscopy (Fig. 1b) is a surface porosity, which was estimated to be of about 5%. These pores are the consequence of both, the oxygen bubbles produced by the reaction between Ti and SiO_2

Table 1 Chemical composition of the glass coating

Comp. (wt%)	SiO_2	CaO	Na_2O	MgO	P_2O_5	K_2O
6P64	64.1	11.6	9.8	6.3	6.0	2.7

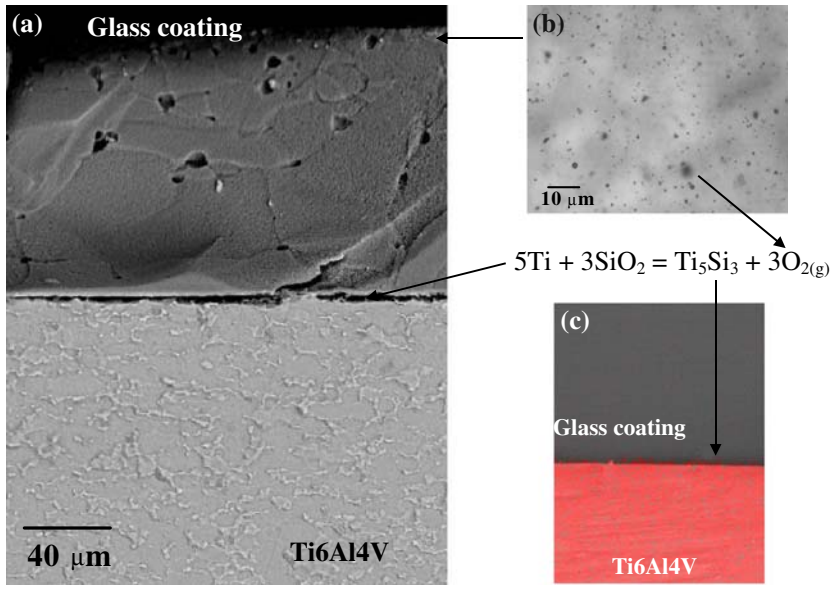

Fig. 1 Microstructural features of the coating: (**a**) Cross-section polished and etched; (**b**) Top view; (**c**) Cross-section polished including an energy dispersive spectrometry (EDS) mapping of Ti (highlighted in red)

at the interface to generate an interfacial layer of Ti_5Si_3 nanoparticles [18], and the air trapped between the glass particles after sintering. The coating cross-section (Fig. 1c) shows that the pores are mostly located at the top of the coating which implies that the main source is the air trapped during processing, because the bubbles from the interfacial layer are typically larger and located at the bulk of the coating, and they are associated to longer firing times [9]. The microstructure observed by scanning electron microscopy (SEM) of the cross-section after acid etching (10 ml HNO_3, 6 ml HF and 80 ml H_2O) is the result of preferential etching at the boundaries between sintered glass particles due to the higher dissolution rates in these areas (Fig. 1a). Previous studies have reported sodium calcium phosphate, $2.4CaO \cdot 0.6Na_2O \cdot P_2O_5$, as the main crystalline phase in the coatings [9–11], while the microstructure revealed in the substrate (Fig. 1a) is composed by grains of α phase in a matrix of plates of α surrounded by β phase, which is a characteristic of a mill-annealed alloy.

Hertzian contact testing

The roughness parameters of the coating (R_a = average roughness, that is, arithmetic mean deviation of surface height from mean value, and S = mean space between the profile peaks) were measured with a Surftest SV-502 bidimensional surface tester with a diamond stylus. According to the measured parameters (R_{a6P64} = 0.21 μm; S_{6P64} = 110.60 μm), it was considered that the surface of the substrate, polished with diamond suspension of 1 μm particle size, ensures a coating surface suitable to be indented without further polishing. The damage sequence during Hertzian monotonic loading was determined in order to establish an interfacial damage criterion. The indentation tests were carried out with WC-Co spheres using an universal electromechanical Instron testing machine (model 8562) with a 1 kN load cell. The radius of the spheres was 1.25 mm and the applied load rate was 2 Ns^{-1}. The surface damage produced by Hertzian contact was determined by optical microscopy immediately after removing the load, by focusing at the top of the coating and at the interface. Possible residual imprint in the metallic substrate was verified by removing the coating through elastic bending of the specimens.

The cyclic tests were carried out by applying fractions of the critical monotonic load for delamination, P_{Del}, using a servo-hydraulic Instron testing machine (model 8511). The cyclic loads were applied in the form of a sinusoidal wave-form with a frequency, f, equal to 10 Hz. Load ratios ($R = P_{min}/P_{max}$) of 0.2, 0.1 and 0.6 were studied. The damage produced for a given maximum load was inspected after a certain number of cycles by observing the contact surface in the optical microscope. If no delamination was observed, a new test was performed in another location of the coating during a higher number of cycles (about 5%). This process was repeated until delamination could be observed. Once this damage was detected, other tests were done with lower number of cycles (less than 5%) in order to bound the number of cycles for which delamination takes place. The critical number of cycles for delamination (N_d) was defined as the number of

cycles at which at least three tests presented this damage, and two tests with 5% lower number of cycles for which this type of damage did not appear.

The possible plastic deformation of the substrate associated to cyclic contact loading was also verified by separation of the substrate and the coating by bending after local delamination was observed at the glass-metal interface. In order to assess the behaviour of the substrate itself to cyclic contact loading, monolithic specimens of Ti6Al4V were prepared under the same conditions as the substrate and subjected to similar cyclic loads with P_{max} equal to 30, 50 and 80 N, and a load ratio, $R = 0.2$. The aspect of the residual impression after the cyclic test was observed by optical microscopy and the diameter and depth was measured in each case.

Results and discussion

Hertzian indentation damage sequence in the coating during monotonic loading

The different damage modes in the porous glass coating/metallic substrate system studied in this work appeared in the following sequence (Fig. 2):

1. Ring cracking at the top surface of the coating. A pre-existent surface flaw ''runs around'' to form a shallow ring. The surface flaw is located close to the contact perimeter over which acts the maximum stress intensity factor.
2. Cone cracking, formed when the ''ring'' begins to flare out into the frustum of a cone. The trajectory of this crack follows closely the σ_3 one, nearly normal to the principal tensile stress, σ_1, in the *prior* stress field.
3. Radial cracking then appears from the interfacial flaws on the central contact axis due to the maximum biaxial bending stress that acts over this axis which is induced by plastic deformation of the substrate. According to the distribution of the principal elastic shear stress $\tau_{13} = ½ (\sigma_1 + \sigma_2)$ evaluated in terms of the sample depth for a Young modulus range between E_c and E_s, this plastic deformation should begin for a load around 10 N (Fig. 3). Therefore, this is actually the first damage of the system, and it is consistent with the maps obtained by Miranda [20] designed to predict the first interfacial damage, that is, plastic deformation of the substrate or the formation of the radial crack in the coating in monotonic loading.
4. For higher loads, delamination of the coating takes place. In transparent glass coatings, this event can be detected by the appearance of a pattern of colours originated by the decomposed spectra of white light when the interface is focused with the optical microscope (Fig. 2d).
5. Secondary cone crack is generated outside the first cone for higher loads, because the expanding contact circle engulfs the previous cracks. For increasing loads some radial cracks can reach the outer surface of the coating.

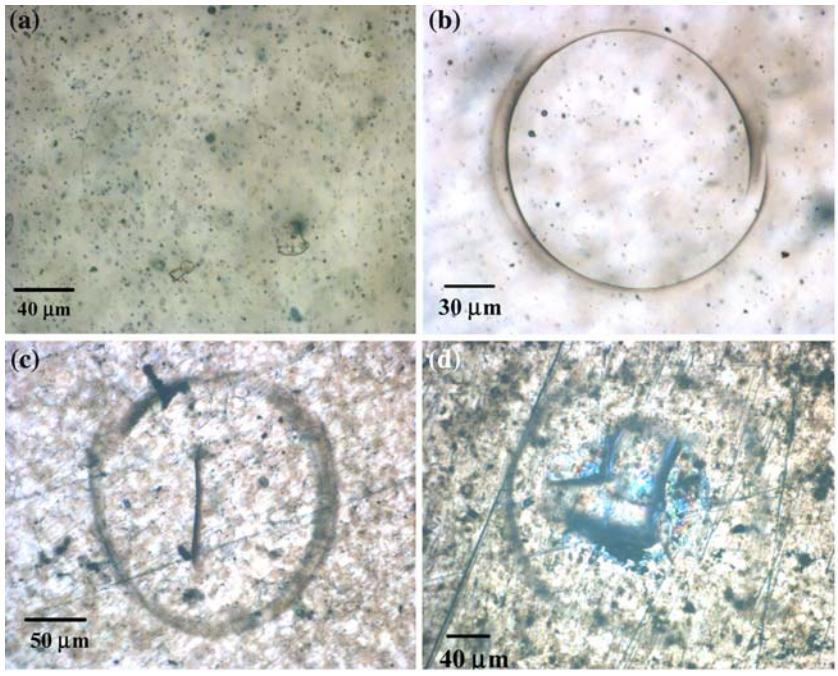

Fig. 2 Optical micrographs of different damages that appear in the coating for increasing Hertzian monotonic loads: (**a**) Ring crack, $P_{rc} = 45 \pm 1$ N; (**b**) Cone crack, $P_{cc} = 48 \pm 1.5$ N; (**c**) Radial crack from the interface, $P_{Rc} = 50 \pm 2$ N; (**d**) Delamination, $P_{Del} = 60 \pm 3$ N

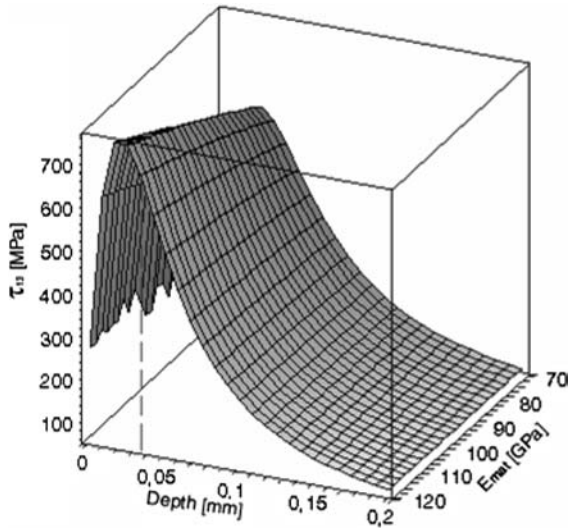

Fig. 3 Principal shear stress distribution ($\tau_{13} = ½ (\sigma_1 - \sigma_3)$ in terms of the coating sample depth for a range of Young modulus between the values of the glass ($E_c = 70$ GPa) and of the Ti6Al4V ($E_c = 110$ GPa). Calculation from the Hertzain stress fields solutions of Huber [19] for $P = 10$ N. Note that the value of τ_{13} which acts on the substrate in the interface (~40 μm, dashed line) is always higher than the Von Mises stress under Hertzian contact for Ti6Al4V ($\tau_{max} = Y/2$, where Y is the yield strength such that $Y_{Ti6Al4V} = 925$ MPa)

Mechanisms of ring and cone crack formation in monotonic contact loading are already well characterized in the literature [21] as well as those corresponding to radial cracks in different bilayer systems [22– 24]. All of them are well known to occur during the loading part of the monotonic test. Delamination in a ceramic/metal system due to Hertzian indentation was first observed by Fisher-Cripps et al. [25] in a Al_2O_3:40 wt% TiO_2 coating on a substrate of steel during monotonic loading. They found that radial cracking was induced during loading, while delamination occurred during the unloading part of the test because of the plastic deformation of the substrate. Here, for a glass/metal system, we have also found that radial cracks are induced before delamination in monotonic loading, although during cyclic loading we have detected delamination before any radial crack can be detected, as it will be discussed in Delamination due to the Hertzian cyclic loading, which is a situation that has not been reported yet.

Delamination is revealed by a pattern of rings of colours, which tend to be better defined as the load is increased (Fig. 4). This can be clearly appreciated in Fig. 4d, where it can be noted that for an applied load of $P = 80$ N the pattern has been completed and it is intersected by previously formed radial cracks. This concentric ring pattern is formed by ''Newton's rings'' that result of the interference between the reflecting waves from two surfaces that are separated by a thin film of variable thickness of a medium with a different refractive index, n, in this case a film of air (low density medium, $n \cong 1$) [26]. The interference is produced between the reflecting wave from the upper surface of the film (glass/air interface) and that one which, after transmitted through the film, is reflected from its lower surface, that is, the latter corresponds to the air/substrate interface if the air film is due to the delamination of the coating. The colours observed are due to the white light used in the present experiments.

From the interference pattern presented in Fig. 4d some features can be extracted from the associated damage: (a) the presence of this colour pattern indicates that there is a narrow gap between the coating and the substrate with a thickness within the interval of wave lengths of the observed colours (400–700 nm) making this possible to observe the interference pattern. In general, this gap shall be of variable thickness. The change in thickness of the coating in the area of contact is too small in order to affect the interference phenomena; (b) the white colour at the outer ring of the pattern together with some blue marks are probably due to a thicker coating/substrate gap which makes interference less effective. On the other hand, the centre of the pattern appears dark because the two surfaces are still in intimate contact without any air gap between them and no reflection (or destructive interference) takes place. The centre is clearly surrounded by the violet colour which means that this area is thinner than the rest of the colour pattern area because corresponds to the smaller wave length of the visible spectra. Therefore, the outer part of the circumferential pattern corresponds to the thicker part of the film and the inner part is thinner. The fact that the colours observed between the centre and the outer of the pattern are not consecutive in the sense of the wave length (violet to red) indicates that the thickness of the gap is clearly irregular. This is observed not only in the radial direction, but also in the tangential direction the colour of the pattern is not constant, which indicates that the gap is also irregular in those zones. Therefore, some fringes of the pattern are not properly ''rings''.

One important point to elucidate is whether plastic deformation of the substrate takes place before delamination during monotonic loading (Fig. 2d). To verify this point, the system was subjected to contact monotonic loading until delamination could be detected (Fig. 2d) and later it was loaded in bending until complete separation of the coating took place. Figure 5 shows the residual indentation imprint on the substrate corresponding to a load of $P_{Del} = 60 \pm 3$ N.

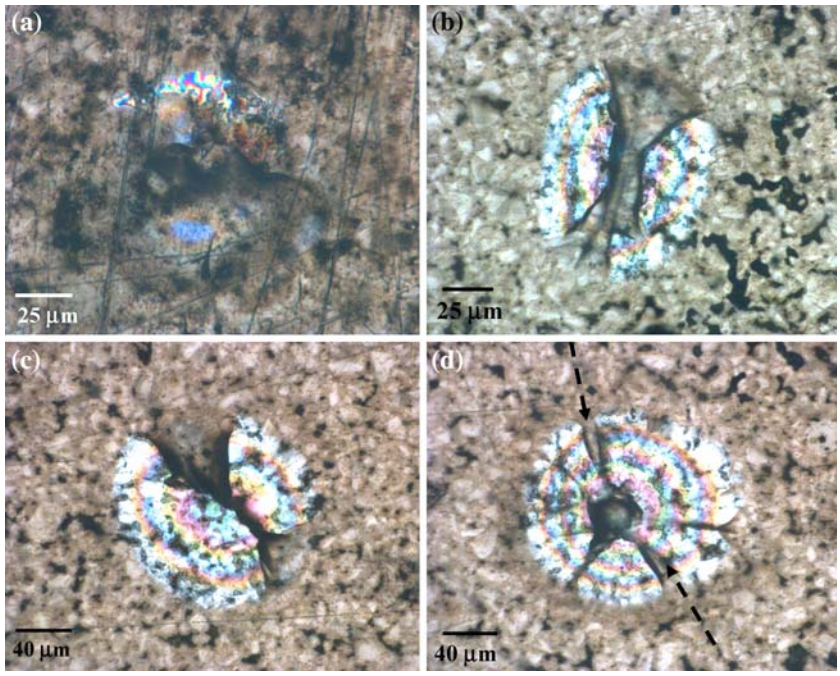

Fig. 4 Evolution of the interference colours pattern due to delamination for increasing Hertzian monotonic loads: (**a**) Critical load for delamination, $P_{Del} = 60 \pm 3$ N, note that the damage is originated from the outer of the substrate imprint; (**b**) $P = 70$ N and (**c**) $P = 75$ N, delamination is clearly increased from the outer up to be arrested by the faces of the radial cracks; (**d**) $P = 80$ N, the colours rings pattern of delamination is completed. Note that, despite there are more radial cracks, there is still some lack of delamination (black dashed arrows)

This shows that there is plastic deformation of the substrate during monotonic contact loading, which is responsible of the posterior delamination of the coating. A possible mechanism associated to delamination in monotonic contact loading is presented in Fig. 6. Once plastic deformation is induced on the surface of the substrate during the loading part, a shear stress appears at the upper points of the imprint because of the elastic mismatch between the coating and the substrate, which could induce the first delamination event at the outer part of the imprint (Figs. 2d, 4a) from a pre-existent interfacial flaw. For increasing loads, there is a larger plastic imprint, as well as more radial cracks, and the incipient delamination tends to form a well defined pattern which goes from the outer to the inner parts of the imprint, until arrested by the radial cracks (Fig. 4b, c). Note that when the load is high enough, the colour ring pattern is completed because there are enough radial cracks to induce delamination in all radial directions (Fig. 4d). There-

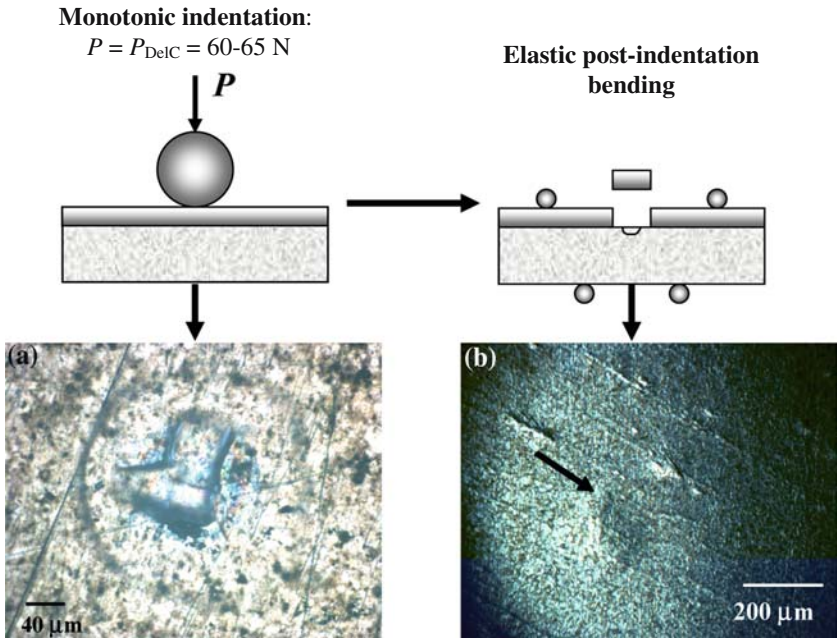

Fig. 5 Post-indentation bending procedure of a coated beam with the purpose to verify the plastic deformation of the substrate associated to delamination: (**a**) Coated specimen with delamination; (**b**) Residual imprint on the substrate observed after removing the coating

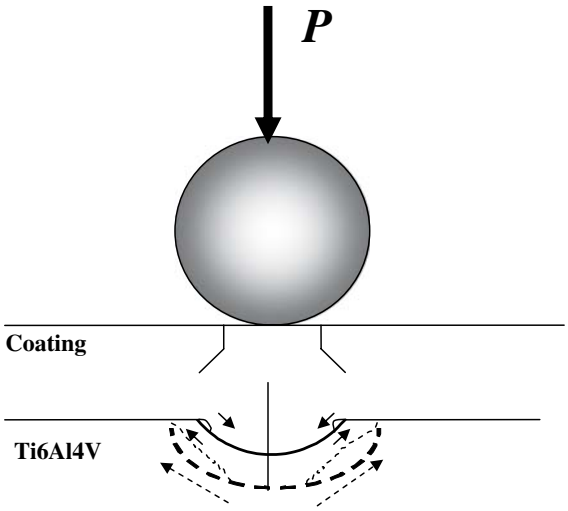

Fig. 6 Mechanism of delamination during the Hertzian monotonic test due to the shear stress induced at the upper points of the substrate imprint. Dashed lines correspond to a higher load than the critical one to produce the first delamination

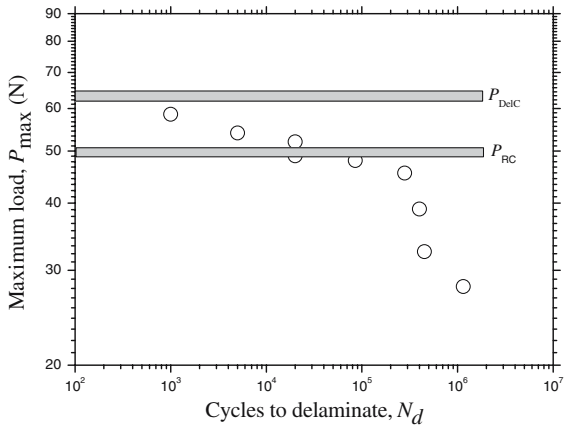

Fig. 7 Maximum applied load, P_{max}, in terms of the number of cycles to delaminate, N_d, during a Hertzian cyclic test for $R = 0.2$. Each N_d value has an uncertainty of maximum 5%

fore, monotonic delamination is initiated and partially completed during the loading part of the test. The role of the elastic recovery of the coating during unloading can be considered small due to the presence of a multicracking damage, i.e. cone and radial cracks.

Delamination due to the Hertzian cyclic loading

The response of the coating to cyclic contact loading was recently studied by the authors [27] by taking ring cracking as the damage criteria. It was observed that, for the same value of maximum applied load, the ring crack under cyclic loading appeared earlier than under static loading. This sensitivity to cyclic loading was attributed to the presence of a microcracked tip damaged zone as a consequence of microfracture of the necks between the glass sintered particles. Following the same methodology, here it is examined the delamination of the coating under Hertzian cyclic loading.

The maximum applied load, P_{max}, in terms of the number of cycles to detect the first delamination at a constant load ratio of $R = 0.2$ is shown in Fig. 7. This curve illustrates that this type of damage is sensitive to Hertzian cyclic loading, that is, it appears at a load smaller than the critical one to detect delamination under monotonic loading, P_{Del}. Note that the curve shows peculiar fatigue behaviour, having two different slopes, with the steeper one occurring at larger number of cycles, with an inflexion point (''knee'') close to the critical load for radial cracking, P_{Rc}. On the other hand, pictures of the top surface and of the interface coating/substrate after delamination in each regime of the curve are depicted in Fig. 8. The top views show that the surface damage in both regimes is similar with the only exception that in the lower slope regime ($P_{max} > P_{Rc}$) there is cone cracking because P_{max} is higher than the critical load for this damage, P_{cc}. The delamination morphology in this regime is also similar as under monotonic loading, showing fringes of different colours with the presence of radial cracks ($P_{max} > P_{Rc}$). However, delamination at $P_{max} < P_{Rc}$, that is, in the high slope regime, is not accompanied by any radial crack and the colour pattern is mostly white and located at the centre of the contact. This indicates that the gap between the coating and the substrate is thick as was noted previously in the outer part of the pattern for monotonic delamination (Fig. 4d). By following the same procedure of post-indentation bending, it was observed that in both regimes there is plastic deformation of the substrate.

The above observations suggest that for $P_{max} > P_{Rc}$ delamination is activated by the presence of radial cracks since they are generated during the first loading cycle and, they increase in number and length with the number of cycles. Besides an intrinsic fatigue mechanism in the coating, it is important to notice that there is an increasing plastic deformation of the substrate, as can be appreciated by measuring the size of the residual imprint on the substrate (Fig. 9). This increment of plastic deformation takes place continuously since the first cycle at decreasing rates until a nearly stable condition is reached (Fig. 10). This may be a manifestation of *cyclic creep* or *ratchetting* which is common in metals when the plastic deformation during the loading portion is not opposed by an equal amount

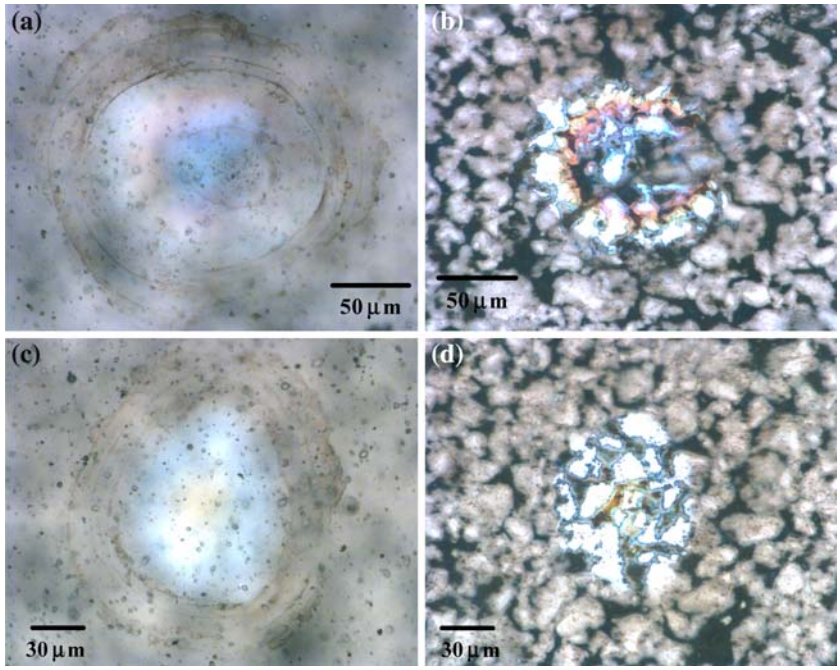

Fig. 8 Damage morphology in the coating under Hertzian cyclic loading: (**a**) and (**b**) Top and interfacial (delamination) views, respectively, for P_{max} = 52 N ($P_{max} > P_{Rc}$) and N_d = 50,000 cycles; (**c**) and (**d**) Top and interfacial (delamination) views, respectively, for P_{max} = 32.5 N ($P_{max} < P_{Rc}$) and N_d = 450,000 cycles

of yielding in the reverse loading direction. The accumulation of damage in ratchetting is accelerated by the mean load as well as by cyclic softening. This cyclic creep effect of the Ti6Al4V alloy was verified by applying Hertzian cyclic loads directly on the substrate for three different maximum load values (30, 50 and 80 N) which already produced residuals imprints observable by optical microscopy during monotonic loading. Figure 9 presents the residual imprints morphologies for increasing loading cycles where it can be observed the difference in diameter and depth. In Fig. 10 the residual imprint diameter is plotted with respect to the loading cycles where it can be appreciated that cyclic creep occurs especially during the first cycles and, afterwards, it tends to saturate. The increase in the plastic deformation of the substrate during cycling may be the reason for inducing secondary rings at the top of the coating (enhanced tensile stress and microfracture of the necks between sintered particles [27]) and an increment in number and length of radial cracks. On the other hand, the degradation of the coating will reduce its capacity of shielding the stress, so that a higher effective stress will be induced on the substrate increasing in this way the surface plastic deformation. Once the cyclic creep becomes stabilized (after about 50000 cycles, see Fig. 10), the increment in the plastic deformation of the substrate is mostly due to an increasing ''effective'' stress at the substrate as a result of continuous degradation of the coating.

On the other hand, for $P_{max} < P_{Rc}$, as well as for the above load range, the increasing plastic deformation of the substrate plays a determinant role in cyclic delamination. In that sense, by considering that the first ring crack appears around 40,000 cycles for P_{max} = 30 N, in spite that there is plastic deformation of the substrate from the first cycle. However, the presence of plastic deformation in the substrate has an important role, since ring cracks in the bilayer system appear at lower cyclic loads than in monolithic materials with the same composition and microstructure as the coating. To which extent the cyclic creep that may occur in the plastic contact zone of the substrate could affect the nucleation of the ring crack is something that has not been investigated. However, as the ring crack appears much later than plastic deformation in the substrate, it seems that this deformation influences ring cracking only by increasing the cyclic effective stress on the substrate, so that it facilitates ring crack nucleation and propagation. In addition, the formation of ring cracks induces an increment in the effective stress on the substrate resulting in further plastic deformation and probably additional cyclic creep (Fig. 10).

Note that it seems that degradation of the coating by some quasiplastic damage below the contact surface does not have an important contribution to the total cyclic degradation. This is supported by the lack of the typical residual mark in the centre of the contact and by the fact that at the depth along the contact axis where the shear stress reaches its maximum value,

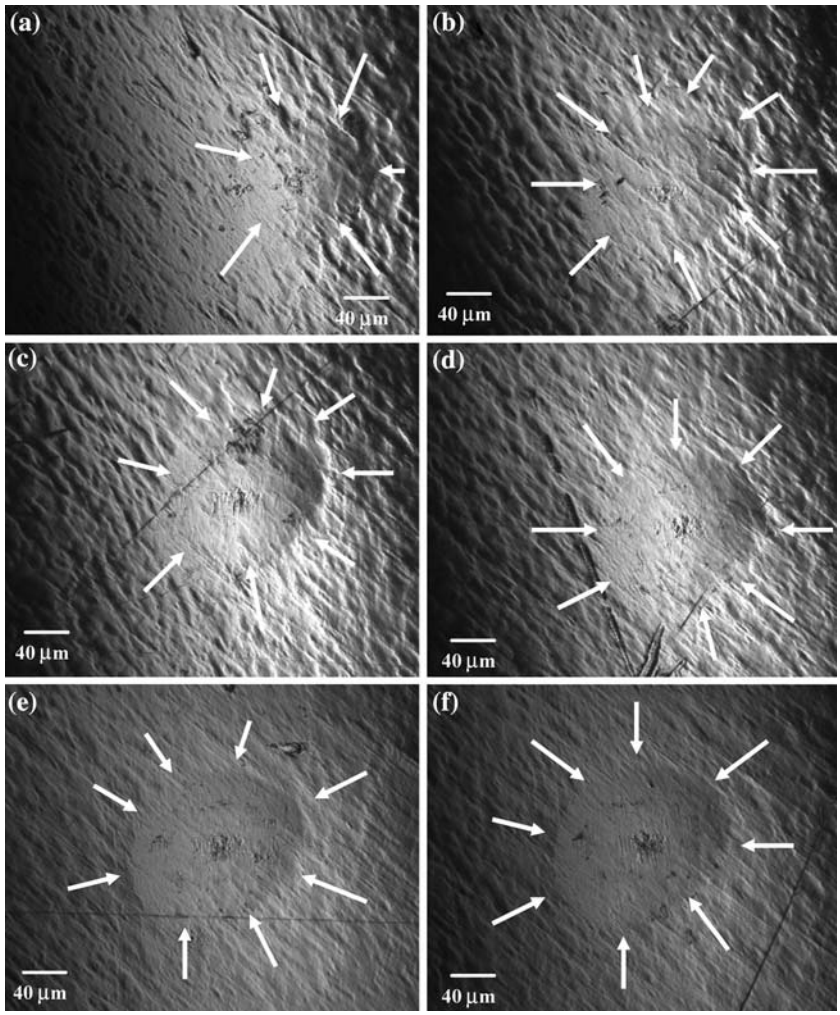

Fig. 9 Residual impression generated on Ti6Al4V alloy during a Hertzian test with P_{max} = 30 N: (**a**) Monotonic test, $N = 1$; (**b**) $N = 10^3$; (**c**) $N = 10^4$; (**d**) $N = 10^5$; (**e**) $N = 2 \times 10^5$; (**f**) $N = 3 \times 10^5$

which is near the interface with the substrate, the initial population of microcracks is smaller than on the contact surface, as can be seen in Fig. 1a.

Additional insight into the mechanisms of delamination under cyclic loading was obtained by investigating the influence of the load ratio, $R = P_{min}/P_{max}$, in the number of cycles for delamination, N_d. The results for R equal to 0.1, 0.2 and 0.6, are shown in the form of plots of log P_{max} vs. log N_d (Fig. 11a) and of log ΔP vs. log N_d (Fig. 11b). It can be noted that for the load range in which $P_{max} > P_{Rc}$ (Fig. 11a) the experimental points obtained at different R values fall on the same single curve, that is, delamination damage is less sensitive to the amount of unloading (weak influence of load ratio) and very sensitive to P_{max}. In the range of $P_{max} < P_{Rc}$ the number of cycles to delamination becomes less sensitive to P_{max}. Besides a larger scatter in the results, not a clear effect of R can be established since the number of cycles to delamination for $R = 0.2$ are equal or shorter than for $R = 0.1$ and $R = 0.6$. On the other hand, by plotting the number of cycles to delamination in terms of ΔP (Fig. 11b), it is clear that the pronounced different behaviour for $R = 0.6$ ($P_{max} > P_{Rc}$) indicates that the damage is mainly influenced by P_{max} and not by ΔP, i.e., in order to have a given number of cycles for delamination, it is only required to fix the value of P_{max} and independently of the value of R. On the contrary, by fixing ΔP the number of cycles for delamination depends strongly on R, because now P_{max} is very different for each value of R.

Therefore, the observations of Hertzian cyclic delamination of the coating could be rationalized by means of different mechanisms acting in each load range (Fig. 12). For the load range where $P_{max} > P_{Rc}$, the first event observed of cyclic delamination is mostly dependent on P_{max} and it could take place because of the growing of an interfacial flaw which is subjected to a cyclic shear stress acting around the perimeter of the imprint (mode II), and which is favoured by the increase in the compliance of the glass because of

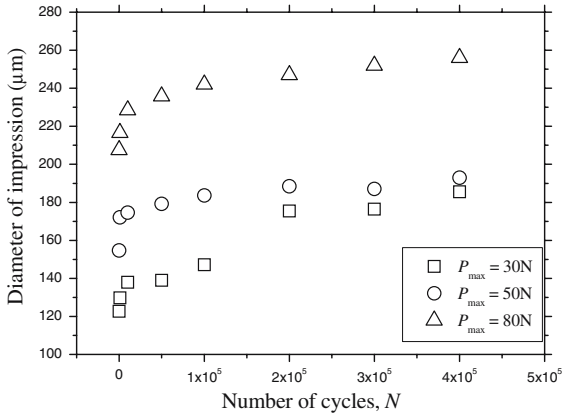

Fig. 10 Change of the mean diameter of the residual impression on the Ti6Al4V alloy with the number of cycles for three different maximum loads

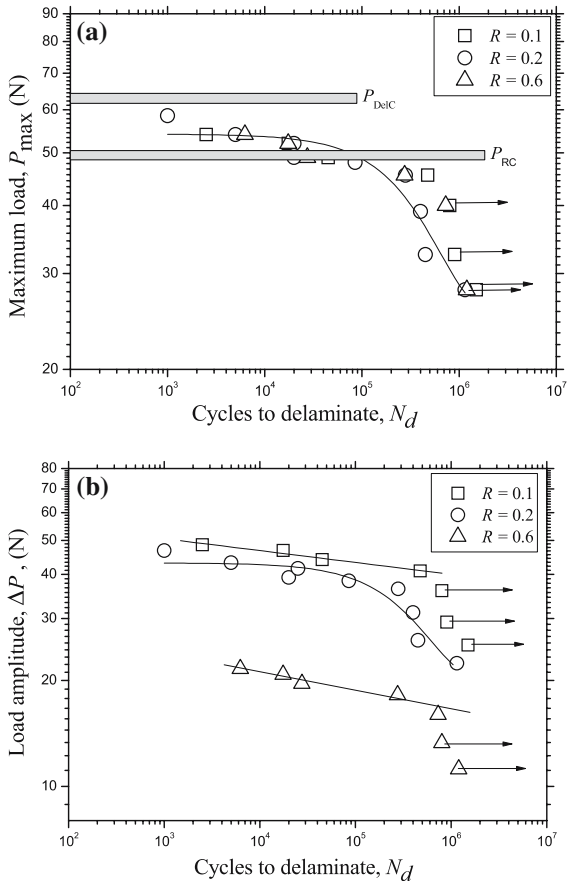

Fig. 11 Influence of the load ratio, R, in the number of cycles to delaminate due to the cyclic loading: (**a**) log P_{max} vs. log N_d and (**b**) log ΔP vs. log N_d. Each N_d value has an uncertainty of maximum 5%

nucleation and extension of multi-radial cracks and increased size of the plastic deformation of the substrate. This makes the delamination pattern to be similar to the monotonic one. This process is directly dependent of the nature of the interface which in this case is composed by the glass with a very thin (~100 nm) interfacial layer of titanium silicide nanoparticles and the metallic substrate. As Hertzian cyclic delamination resistance is more dependent on P_{max}, this inidicates that the growth of this interfacial crack has a typical ceramic-like behaviour, that is, cyclic crack growth is mostly influenced by K_{max} [28, 29]. However, the exact mechanism of cyclic delamination advance is unclear and can be influenced by several other factors as crack-tip plasticity due to the substrate, the presence of the interfacial layer of titanium silicide, or debris wedging effect due to wear shear particles, among others.

For $P_{max} < P_{Rc}$, as no radial cracks are formed, delamination appears to be exclusively dependent of the plastic deformation of the substrate and the subsequent residual stress associated to elastic recovery of the coating during unloading. Therefore, it is proposed that in this load range, delamination is a nucleation and cyclic interfacial crack growth phenomenon and is activated by cyclic unloading stresses. In this regime, there is still some small plastic deformation of the substrate, but, as opposed to the higher load regime, no radial cracks appear in this case. This plastic deformation of the substrate will create a residual stress at the glass/metal interface (mode I), because points of the coating located there are not able to go back to their original positions once unloading. Therefore, this residual stress may be also sensitive to unloading, that is, to the value of R. In addition, the plastic deformation at the surface of the substrate is increased with the number of cycles by cyclic creep. The shear stress which is induced near the border of the imprint makes flaws grow, which finally could induce delamination during unloading part. Therefore, within this load range, cyclic delamination progresses basically under cyclic mode I and the mechanism of this interfacial crack growth could involve the process of alternating crack-tip blunting and sharpening of the initial delamination mark similar to what was reported by McNaney et al. [30] in their analysis of the interfacial cyclic crack-growth of Al/Al_3O_3 bimaterial sandwich samples. Such a mechanism could be consistent with the dependence of the number of cycles to delamination with K_{max} or ΔK in this load range (Fig. 11). It is clear that also the fatigue mechanism in this load range can be influenced by other factors and further analysis of the separated faces after cyclic delamination is required in order to verify these assumed mechanisms for both regimes.

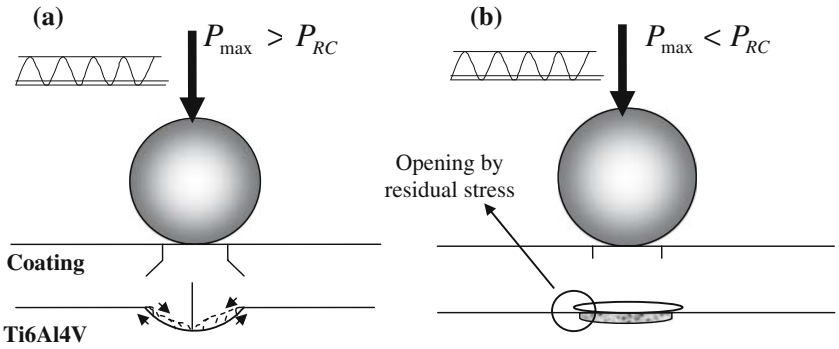

Fig. 12 Proposed mechanisms of delamiantion due to the Hertzian cyclic loading depending on the maximum applied load range: (**a**) $P_{max} > P_{Rc}$ where the delamination is associated to the shear stress induced at the outer of the imprint which acts on an interfacial flaw and promotes its growing up to find the faces of the radial crack (dashed lines); (**b**) When $P_{max} < P_{Rc}$ the small plastic deformation of the substrate promotes the driving force for crack growth because of the residual stress induced at the interface

Conclusions

The mechanical response of the interface of the glass-based coating on Ti6Al4V under monotonic and cyclic Hertzian loading has been studied and the main conclusions can be summarized as follows:

1. Under Hertzian monotonic loading the damage sequence starts with three brittle damage events (ring, cone and radial cracking) followed by coating delamination, which is associated with the shear stress induced by the plastic deformation imprint of the substrate and the presence of radial cracks as a result of the flexure effect at the bottom surface of the coating.
2. It has been shown that delamination damage is sensitive to Hertzian cyclic loading, which appears for a maximum cyclic load lower than the critical one under monotonic conditions. The plastic deformation of the substrate during the first cycle and its increment during the subsequent number of cycles because of cyclic creep (ratchetting), play a determinant role in Hertzian cyclic delamination of the coating. Further cyclic degradation of the coating by secondary rings in the low load regime and also with radial cracks in the higher load regime, induce a higher effective stress on the substrate with a subsequent increment of the cyclic plastic deformation.
3. Two different cyclic delamination regimes associated with different damage morphologies were found for different load ranges. They are characterized by the presence of radial cracking and by its sensitivity to the maximum load. For the high load regime, this behaviour is explained in terms of the shear stresses enhanced by radial crack, both originated by cyclic deformation of the substrate and degradation of the coating, meanwhile, for the low load regime, delamination is the consequence of the residual stress induced at the interface due to both elastic recovery of the coating and cyclic deformation of the substrate.

Acknowledgements This work is supported by the Spanish Ministry of Science and Technology through Grant No. MAT202-00368, the Generalitat de Catalunya through the Gaspar de Portolà exchange program, and the National Institutes of Health/National Institutes of Dental and Craniofacial Research through Grant No. IR01DE11289. The authors would like to thank specially Dr. Luis Llanes for valuable discussion. Finally, J. Pavón wishes to thank Colciencias-Colombia for financial sponsorship of his Ph.D. studies.

References

1. Hench L (1991) J Am Ceram Soc 74:1487
2. Ducheyne P, Hench L, Kagan A, Martens M, Burssens A, Muller JC (1980) J Biomed Mater Res 14:225
3. Xue W, Tao S, Liu X, Zheng XB, Ding C (2004) Biomaterials 25:415
4. Gu YW, Khor KA, Cheang P (2003) Biomaterials 24:1603
5. Lacefield WR (1993) An introduction to bioceramics. World Scientific, Singapore, p 223
6. Chern Lin JH, Shen KS, Ju CP (1995) Mater Chem Phys 41:82
7. Hench L, Anderson Ö (1993) An introduction to bioceramics. World Scientific, Singapore, p 239
8. Donald IW (1993) J Mater Sci 28:2841
9. Gómez-Vega JM, Saiz E, Tomsia AP (1999) J Biomed Mater Res 46:549
10. Pazo A, Saiz E, Tomsia AP (1998) Acta Mater 46:2551
11. Pazo A, Saiz E, Tomsia AP (1998) Ceramic microstructures: control at atomic level. Plenum Press, Berkeley, p 543
12. Hench L, Splinter RJ, Allen WC, Greenlee TK (1971) J Biomed Res Symp 2:117
13. Brunski JB (1992) Clinic Mater 10:153
14. Lawn BR (2002) Curr Opin: Solid State Mater Sci 6:229

15. DeLong R, Douglas WH (1983) J Dent Res 62:32
16. Eberhardt AW, Lewis JL, Keer LM (1991) ASME J Biomed Eng 113:410
17. Lopez-Esteban S, Saiz E, Fujino S, Oku T, Suganuma K, Tomsia AP (2003) J Eur Ceram Soc 23:2921
18. Oku T, Suganuma K, Wallenberg LR, Tomsia AP, Gomez-Vega JM, Saiz E (2001) J Mat Sci: Mat Med 12:413
19. Huber MT (1904) Ann Phys (Leipzig) 43:153
20. Miranda P (2003) Diseño de Materiales Multicapa Resistentes al Daño por Contacto, Ph.D. Thesis. Universidad de Extremadura, p 150
21. Frank FC, Lawn BR (1967) Proc R Soc Lond A 299:291
22. Warren PD (1995) J Eur Ceram Soc 15:201
23. Chai H, Lawn BR, Wuttiphan SJ (1999) J Mat Res 9:3805
24. Rhee YW, Kim HW, Deng Y, Lawn BR (2001) J Am Ceram Soc 84:1066
25. Fisher-Cripps AC, Lawn BR, Pajares A, Wei L (1996) J Am Ceram Soc 79:2619
26. Hecht E, Zajac A (1974) Optics. Addison-Wesley, Massachusetts, p 293
27. Pavón J, Jiménez-Piqué E, Anglada M, Saiz E, Tomsia AP (2006) Acta Mater, in press
28. Suresh S (1998) Fatigue of materials. Cambridge University Press, Cambridge, p 113
29. Ritchie RO (1999) Int J Fract 100:55
30. McNaney JM, Cannon RM, Ritchie RO (1996) Acta Mater 44:4713